2004

Sol-Gel Derived Pt-Ir Mixed Catalysts for DMFC Applications

Birss, Viola I.; Tsaprailis, Haralampos

The Electrochemical Society

Tsaprailis, Haralampos and Birss, Viola I. (2004). "Sol-Gel Derived Pt-Ir Mixed Catalysts for DMFC Applications". Electrochemical and Solid State Letters, Vol. 7(10): A348-A352.
http://hdl.handle.net/1880/44727
journal article

Electrochemical and Solid-State Letters, **7** (10) A348-A352 (2004)
1099-0062/2004/7(10)/A348/5/$7.00 © The Electrochemical Society, Inc.

Sol-Gel Derived Pt-Ir Mixed Catalysts for DMFC Applications

Haralampos Tsaprailis* and Viola I. Birss,z**

Department of Chemistry, University of Calgary, Calgary, Alberta, Canada, T2N 1N4

Thin, nanoparticulate films of Pt-Ir (1.8:1 molar ratio), formed using a sol-gel derived process, show excellent activity toward methanol oxidation at room temperature for use in direct methanol fuel cells (DMFCs). When compared on a mass basis to pure Pt or Ir sol-based films, $Pt_{1.8}Ir$ yields 3.5 and 6 times higher methanol oxidation activity, respectively, and is also significantly more active than carbon-supported Johnson-Matthey PtRu (1:1). When also corrected for true surface area, the $Pt_{1.8}Ir$ catalyst continues to outperform Pt and exhibits excellent stability. The Pt-Ir catalyst is most active when dried at 250°C, and conversion of Ir to Ir oxide causes significant loss in methanol oxidation activity.
 [DOI: 10.1149/1.1792253]

Manuscript submitted January 12, 2004; revised manuscript received March 31, 2004. Available electronically September 15, 2004.

In a fuel cell, the anode catalyst provides the foundation for converting the chemical energy of the fuel into electrical energy. Pt is the best anode for hydrogen oxidation, but when methanol is used as the fuel, CO, formed as a reaction intermediate, irreversibly adsorbs to the Pt surface, rapidly lowering its activity.[1,2] The most active material identified to date for methanol oxidation is the Pt/Ru bifunctional catalyst, with Ru believed to serve the role of removing $CO_{(ads)}$ from the Pt sites as $CO_{2(g)}$,[3] as shown in

$$\text{Ru-OH}_{(ads)} + \text{Pt-CO}_{(ads)} \rightarrow \text{Ru} + \text{Pt} + \text{CO}_{2(g)} + \text{H}^+ + \text{e}^- \quad [1]$$

Most of the published literature indicates that metallic Ru is preferred in this reaction,[4-7] while some groups have proposed that Ru oxide is the active species.[3,8] The majority of direct methanol fuel cell (DMFC) anode catalyst research has focussed on binary Pt-Ru catalysts, with less attention having been paid to other binary, or ternary/quaternary catalyst development. Successful fabrication of these new catalysts requires controlled mixing of the desired components at the nanoscopic level.

Our previous research has been directed towards the formation of nano-sized sols of Pt,[9] Ir,[10] NiO_x,[11] and CoO_x[11] using "sol-gel" (SG) synthesis. In metals that readily form oxides, these particles undergo hydrolysis to form a cross-linked polymer or [sol] gel structure. However, in Pt and Ir, the nanoparticles remain metallic in nature, as verified by their distinctive cyclic voltammetric (CV) signatures, and from X-ray diffraction (XD), X-ray photoelectron spectroscopy (XPS) analysis.[9,10,12,13] One of the key benefits of these synthetic routes is the ability to mix materials at the atomic scale.

We have employed these methods and materials to form, for the first time, nanoparticulate binary mixtures containing Pt and Ir, in controlled ratios. Pt-Ir mixtures have been previously formed using electrodeposition methods,[14] solution phase reduction,[15] and by precipitation techniques.[16] Although Ir promoted methanol oxidation when coupled with Pt,[16] all three previous studies have reported that the combination of Pt and Ir is less active toward methanol oxidation than the PtRu analog.

In the present work, Pt-Ir catalysts, with atomic ratio of 1.8:1 Pt:Ir, are shown to exhibit excellent activity toward methanol oxidation and very good tolerance towards CO adsorption. Furthermore, it is demonstrated that when the Ir component was maintained in the metallic state, a significantly higher activity is seen versus when Ir is electrochemically oxidized.

Experimental

Pt and Ir sol synthesis.—Pt and Ir sols were prepared as previously reported in the literature.[9,10] The metal salt precursors, H_2PtCl_6 (>37.5% metal basis, 99.9% pure, Aldrich) and anhydrous $IrCl_3$ (Aldrich), were added to two and three parts, respectively, of sodium ethoxide (96%, Aldrich), and then dissolved in 10 mL of absolute ethanol (>99.5% pure, Aldrich). The precursor solutions were then refluxed for ~2 h and then stirred at room temperature for ~20 h, all under an argon atmosphere (Praxair). The suspensions were then filtered to remove the precipitate (NaCl).

Compositional analysis of mixed Pt-Ir sols.—The preparation of the mixed Pt-Ir sol involved combining the individual sols in a presumed 1:1 molar ratio, assuming complete conversion of starting material into the sol phase. The true molar ratio of Pt:Ir in the mixed Pt-Ir sols was determined by dissolution and subsequent analysis using a Thermo Jarrell Ash model AtomScan 16 inductively coupled plasma atomic emission spectrophotometer (ICP-AES). The desired sols were micropipetted into 10 mL volumetric flasks and digested with 0.5 mL of aqua regia, prepared using ACS grade reagents (Aldrich), for 48 h. The digested sols were then diluted using Mega-Pure water (ACS grade, Corning) and emissions were collected at 265.9 nm and 224.3 nm for Pt and Ir, respectively.

Electrode preparation and testing.—Au electrode substrates were chosen due to their relatively inert electrochemical response in 0.5 M H_2SO_4 and low affinity toward methanol oxidation. Clean glass slides were first sputter-coated with a ~10 nm layer of Ti for adhesive purposes, followed by a ~120 nm coating of Au, using a Denton DV-502A high vacuum sputterer. All Pt, Ir, and Pt-Ir sols were deposited on these Au-coated slides using micropipette deposition and then dried between 50 and 500°C in air.

Electrochemical experiments were conducted using a two-compartment cell containing 0.5 M H_2SO_4 (ACS grade, Aldrich), deaerated with N_2 (Praxair) by passing it initially through the cell solution and then over it during data collection. A saturated sodium calomel electrode (SSCE, 0.237 *vs.* SHE) served as the reference electrode and was placed in one compartment, while the sol-coated Au substrate, the working electrode (WE), was located in the second compartment. This compartment also contained the high surface area Pt gauze (99.9% pure, Alfa Aesar) counter electrode. In this paper, all current densities are given with respect to both geometric and real surface areas of the WE, as indicated, and are also corrected for the total catalyst loadings, while all potentials are reported *vs.* the SHE. Powerlab/200, running Chart for Windows v4.0.1, was used to acquire data from the Hokuto-Denko HA-301 potentiostat, controlled by an EG&G PARC model 175 universal programmer. Methanol oxidation was conducted on Pt, Ir, and Pt-Ir sol catalysts, as well as at carbon-supported PtRu catalyst (1:1, Johnson Matthey, 1 mg/cm^2 Pt loading), in a stirred 1 M methanol (ACS grade, Aldrich) and 0.5 M H_2SO_4 cell solution. Upper potential limits and all other conditions were kept constant between samples and data were not compensated for solution resistance.

Morphology and compositional mapping of Pt-Ir films.—The morphology of the Pt-Ir coating was determined using a JEOL JXA-8200 electron microprobe (EMPA), coupled with a wavelength-

* Electrochemical Society Student Member.
** Electrochemical Society Active Member.
z E-mail: birss@ucalgary.ca

Table I. Pt and Ir content in mixed SG-derived Pt-Ir thin films using ICP-AES.

Sample	Pt[a] (ppm)	Ir[a] (ppm)	Molar ratio Pt:Ir
1	24.0	13.1	1.80
2	25.1	13.5	1.83
3	24.7	13.4	1.82
4	24.2	13.2	1.81
Average	24.5	13.3	1.82
Standard deviation	0.5	0.2	0.01
Theoretical maximum[b]	24.5	29.2	—
Conversion efficiency	98-100%	44-46%	—

[a] Emissions collected at 265.9 nm and 224.3 nm for Pt and Ir, respectively.
[b] Anticipated metal content based on the amount of starting materials employed.

dispersive X-ray spectrometer (WDS) for compositional analysis. A Rigaku multiflex diffractometer (XRD), equipped with JADE XRD pattern processing (Release 6.5), was used for compositional and particle size analysis of Pt-Ir samples dried at 200°C for 15 min. Particles sizes were confirmed using a Hitachi H-7000 transmission electron microscope (TEM, Microscopy and Imaging Facility, University of Calgary), with an acceleration voltage of 75 kV.

Results and Discussion

Compositional and structural characterization of Pt-Ir catalyst.—The bulk composition of the mixed Pt-Ir sols, prepared by combining the individual Pt and Ir sols in a 1:1 ratio, was determined to be approximately 1.8 moles of Pt to 1 mole of Ir using ICP-AES (Table I). Therefore, the binary catalyst is referred to as $Pt_{1.8}Ir$ in the present work. The conversion efficiency is a measure of the amount of metal (Pt or Ir) present in the sol *vs.* the anticipated content based on the amount of starting materials employed. Based on the ICP data (Table I), the conversion efficiency of Pt was found to be 98-100%, while for Ir, it was only ~45%. This is consistent with the dark color of the precipitate, anticipated to be primarily NaCl,[12] formed in the Ir sol synthesis, indicating some co-precipitation of Ir and/or Ir oxide.[13] In contrast, the precipitate formed in the Pt sol synthesis was generally white, and sometimes greyish in color, demonstrating that the majority of the Pt remained in the solution phase.

To establish the morphology of the catalyst, $Pt_{1.8}Ir$ sol was aliquot-deposited on Au substrates, dried at 200°C for 15 min under atmospheric conditions, and then examined after electrochemical testing using EMPA. The secondary electron image (Fig. 1a) of the mixed metal catalyst shows a mud-cracked structure, typical of hydrous or sol-derived materials.[17,18] As the $Pt_{1.8}Ir$ coatings likely contain solvent species when placed in the high-vacuum environment, rapid film drying may cause stress within the film and subsequent film cracking. When electrodes that had not been subjected to electrochemical testing were examined, the films had a very similar appearance. That the films are very stable electrochemically suggests that the cracked morphology is induced by the vacuum environment, and is not present in freshly formed films under normal atmosphere conditions.

The backscattered image (Fig. 1b) shows no contrast in atomic density, suggesting a homogeneous distribution of Ir and Pt, which is consistent with the Pt and Ir elemental maps, obtained using WDS. The Pt and Ir elemental counts were standardized to allow for direct comparison, showing ~1.8 times as much Pt (highest count % = 10) in the coating *vs.* Ir (highest count % = 5.5). The post-electrochemical analysis of the bulk composition of the $Pt_{1.8}Ir$ coatings using WDS was in good agreement with pre-electrochemical analysis using ICP-AES. WDS profiling for oxygen, not shown here, came up negative, strongly suggesting the absence of oxide formation. Therefore, the composition of the $Pt_{1.8}Ir$ coatings appears to remain unchanged at a molar ratio of *ca.* 1.8 mol of Pt per mole of Ir during electrochemical experimentation. Furthermore, consistent with the backscattered image, the elemental maps show that Pt and Ir are homogeneously distributed within the sol coating, at least on the micron scale.

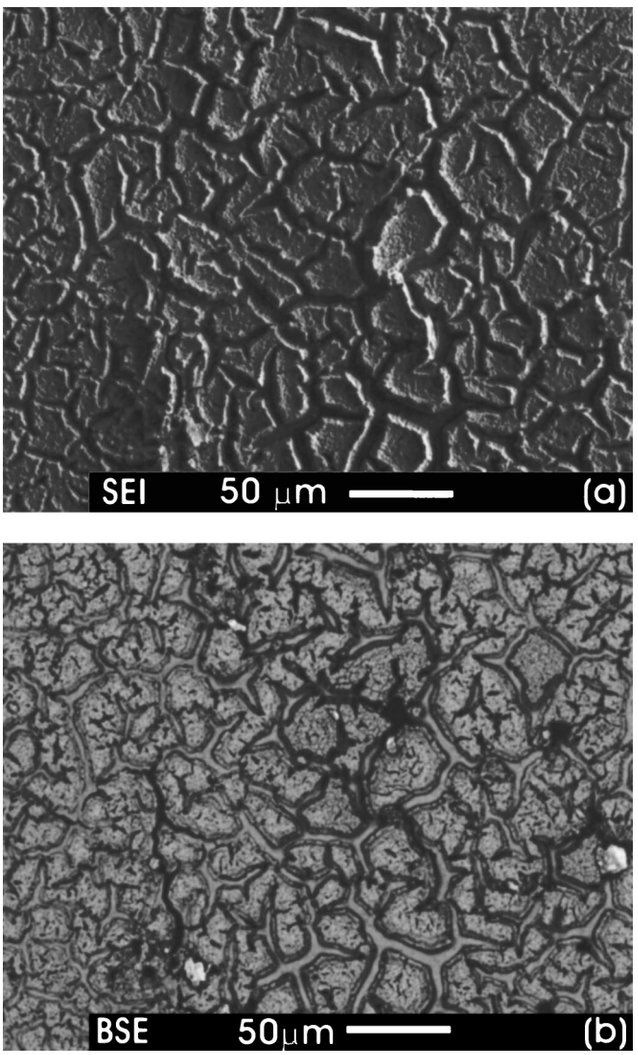

Figure 1. EMPA images of $Pt_{1.8}Ir$ coated Au substrate, dried at 200°C/15 min, after electrochemical testing; (a) secondary electron image and (b) backscattered image.

XRD analysis of the $Pt_{1.8}Ir$ catalysts, dried at 200°C for 15 min in air, was also carried out to confirm the film composition (Fig. 2). It can be seen that both Pt and Ir are present in the dried sols, as is the sol by-product, NaCl. 2θ values of the $Pt_{1.8}Ir$ sol powder do not overlap precisely with the literature values for Pt and Ir, but lie between the two reference lines. This may be the result of the closeness of these lines or, similar to the case of PtRu catalysts,[19,20] this may indicate that the Pt and Ir nanoparticles are partially or fully alloyed. Furthermore, the XRD patterns do not indicate the presence of Pt or Ir oxide in the freshly formed catalyst, consistent with the absence of a CV response characteristic of these phases. The average particle size determined from the XRD peak widths for Pt and Ir using the Scherrer equation[21] is <4 nm, consistent with published results for Ir (1-2 nm)[12] and Pt (1-3 nm)[9] sols formed using our methods. The XRD derived particle sizes data were confirmed using

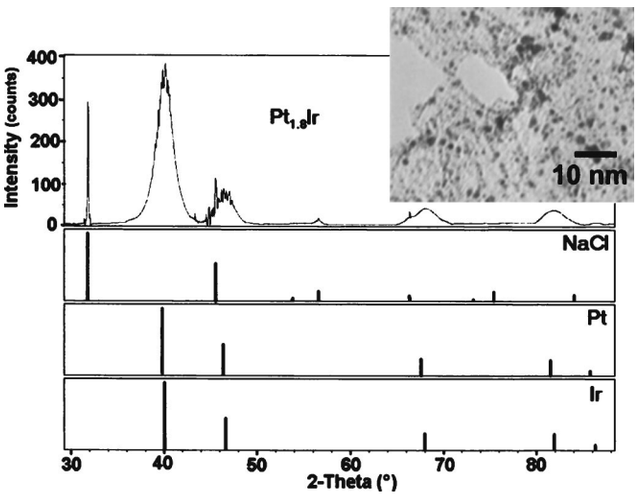

Figure 2. XRD data for $Pt_{1.8}Ir$ sol dried at 200°C for 15 min. Inset: Pre-electrochemistry, TEM image of $Pt_{1.8}Ir$ films (150,000×).

TEM (Fig. 2 inset), showing particle sizes in the range of 1.5 to 3.5 nm.

Electrochemical behavior of $Pt_{1.8}Ir$ thin films.—Figure 3 shows the CV response of thin films of the mixed $Pt_{1.8}Ir$ catalyst, as well as those of the pure Pt and Ir sol components, in 0.5 M sulfuric acid. These three coatings were deposited concurrently to minimize sol aging effects and allow good comparison between them. In each case, a 40 μL aliquot of the sol was deposited on the Au electrode surface and the electrodes were then dried at 200°C/air for 15 min. The potential was cycled until a steady-state CV response was obtained. Electrochemical analyses did not indicate surface oxide formation for any of these electrodes. Therefore, as previously reported,[9,10] the films formed in air are composed of metallic Pt and Ir. The current density in each case has been corrected for the metal content of the film (based on the ICP results). The CV response of the Au substrate, being just due to double layer charging in this potential range, is not detectable at the current sensitivity employed here and therefore is not shown in Fig. 3.

Note that the hydrogen underpotential deposition (H_{upd}) region for the pure Pt film is significantly smaller in magnitude than for pure Ir. This should be the reverse, based on the reported H_{upd} charges anticipated for Pt (0.22 mC/cm^2)[22] and Ir (0.1365 mC/cm^2)[23,24] and also when considering the fact that the real Pt content of the film is approximately twice that of Ir. This suggests that the Pt particles are larger (lower surface area) than are the Ir particles or that their distribution is not yet optimized.

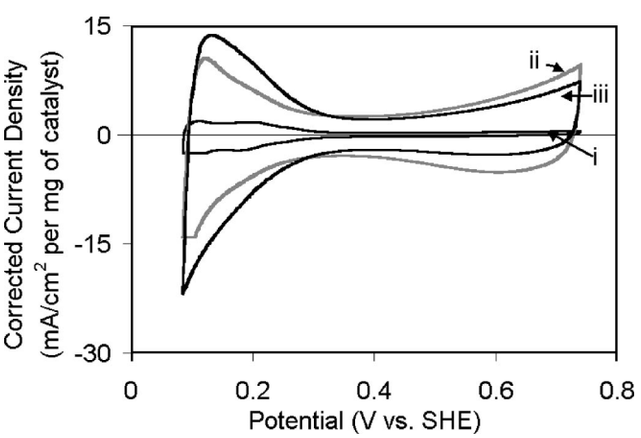

Figure 3. CV profiles of (i) Pt, (ii) Ir, and (iii) $Pt_{1.8}Ir$ sols dried at 200°C/15 min. Au substrate not detectable on this current scale. (Deaerated 0.5 M H_2SO_4, 20 mV/s.)

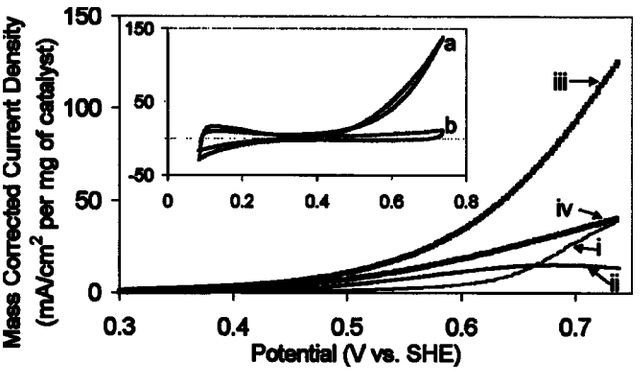

Figure 4. Methanol oxidation data at (i) Pt, (ii) Ir, and (iii) $Pt_{1.8}Ir$ sols corrected for geometric area and catalyst loading. Sols were dried at 200°C for 15 min. (iv) PtRu (1:1) dispersed on carbon was obtained and used as received from Johnson Matthey. Only the first CV sweeps are shown (1 M Methanol + 0.5 M H_2SO_4, 20 mV/s). Inset: $Pt_{1.8}Ir$ (a) with and (b) without methanol present.

The $Pt_{1.8}Ir$ CV profile response appears similar to that of pure Ir. Furthermore, when the integrated H_{upd} charges for Pt and Ir (120 and 366 mC/cm^2 per mg metal, respectively) are summed in a ratio of 1.8 Pt: 1 Ir, the H_{upd} charges should be ~210 mC/cm^2 per mg catalyst. However, the value obtained for the $Pt_{1.8}Ir$ catalyst is close to twice this value, ~400 mC/cm^2 per mg of catalyst. The higher $Pt_{1.8}Ir$ H_{upd} charge indicates a better distribution of the Pt and Ir particles when mixed together, a reduced Ir particle size, or some other synergistic effect caused by the mixing together of the Pt and Ir sols. In addition, the mixing of Pt and Ir sols leads to the improved utilization of the materials, as seen by the fact that $Pt_{1.8}Ir$ displays a significantly higher raw current per milligram signal than its individual components. Furthermore, the CV response of the mixed metal film was extremely stable to potential cycling, indicative of a stable structure and good film adhesion.

Methanol oxidation at Pt, Ir, and $Pt_{1.8}Ir$ sols dried at 200°C.—The activity of the $Pt_{1.8}Ir$ catalyst toward methanol oxidation was established using a range of sweep rates and was compared to that at the pure Ir and Pt sol-formed films, as well as to a commercial carbon-support PtRu catalyst. In all cases, the CV response in 0.5 M sulfuric acid was subtracted from that in 1 M methanol + 0.5 M sulfuric acid, as shown in Fig. 4 (inset) for the $Pt_{1.8}Ir$ catalyst. A comparison of the activity of all of materials under study, after an analogous baseline subtraction, as well as correction for geometric area and catalyst loading, is shown in Fig. 4. To prevent Pt or Ir oxide formation, the upper potential was again not allowed to exceed 0.75 V *vs.* SHE in these experiments.

Excellent methanol oxidation activity is seen for the $Pt_{1.8}Ir$ catalyst, independent of sweep rate, with the onset of oxidation occurring at ~0.27 V *vs.* SHE. $Pt_{1.8}Ir$ methanol oxidation currents (at 0.7 V *vs.* SHE) were 3.5 and 6 times higher than at the pure Pt and Ir sol-based films, on a mass basis, respectively. More important, when compared to the Johnson-Matthey PtRu (1:1) catalyst, $Pt_{1.8}Ir$ outperformed the PtRu catalyst by a factor of 2.7 in current density (at 0.7 V *vs.* SHE), at room-temperature conditions. The PtRu catalyst was supported on high surface area carbon that is intended to maximise the distribution of PtRu particles, thus increasing the area available for catalysis. In contrast, the $Pt_{1.8}Ir$ catalyst was deposited on a relatively smooth Au surface that would not be expected to generate the optimum catalyst distribution. Also, it is unlikely that all of the $Pt_{1.8}Ir$ catalyst particles would be in good electrical contact

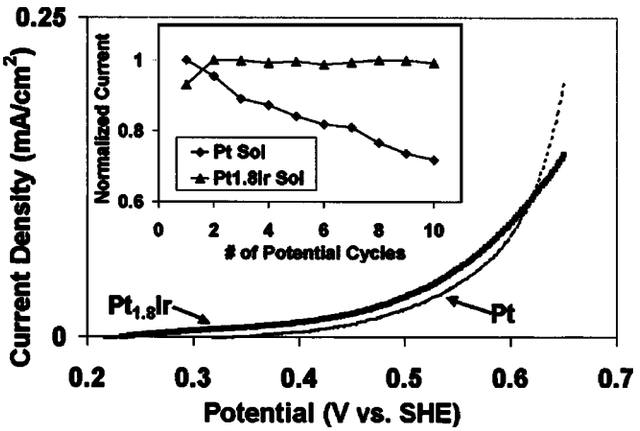

Figure 5. Methanol oxidation data at Pt and $Pt_{1.8}Ir$ sols corrected for real H_{upd} areas. Sols were dried at 200°C for 15 min. Only first CV sweeps are shown [1 M Methanol + 0.5 M H_2SO_4, 20 mV/s]. Inset: Stability of normalized methanol oxidation currents measured at constant potential (0.65 V *vs.* SHE) as a function of CV cycle number.

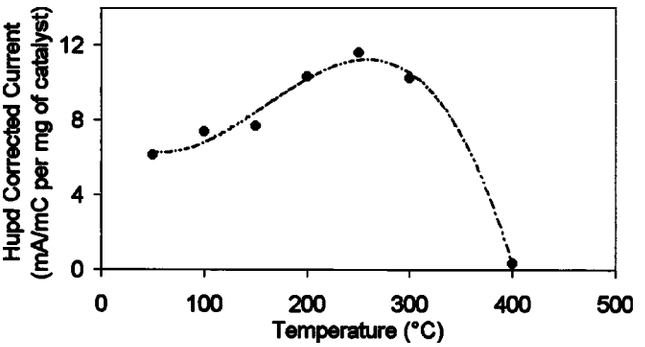

Figure 6. Effect of drying temperature on methanol oxidation currents corrected for real area at $Pt_{1.8}Ir$ thin films. Drying time is 15 min. (Stirred 1 M Methanol + 0.5 M H_2SO_4, 20 mV/s).

with the smooth Au substrate or with each other. Therefore, it is anticipated that $Pt_{1.8}Ir$ would be still more catalytic toward methanol oxidation when distributed on a high surface area support such as carbon, conditions under which the utilization efficiency of the $Pt_{1.8}Ir$ particles would be maximized. These types of experiments are currently underway.

Figure 5 shows the methanol oxidation data of Fig. 4 on a true active surface area basis, as gauged from the magnitude of the H_{upd} peaks. It can be seen that the $Pt_{1.8}Ir$ catalyst still outperforms pure Pt, especially at potentials below 0.65 V, while the pure Ir sol remains the least active. Another significant advantage of our $Pt_{1.8}Ir$ catalyst is that there is no loss in methanol oxidation activity with repeated CV cycling (Fig. 5, inset), in contrast to the case at the Pt sols, where the current drops irreversibly in the presence of methanol after only a few cycles of potential. At $Pt_{1.8}Ir$, the current remains unchanged during cycling and any losses experienced at constant anodic potentials are immediately regained upon resumption of the potential sweep. As discussed earlier, CO poisoning of Pt alone greatly diminishes methanol oxidation currents because CO irreversibly adsorbs to its surface, blocking the active sites. The role of Ru in PtRu catalysts is to remove adjacent adsorbed CO from Pt. The excellent activity and especially the stability of our $Pt_{1.8}Ir$ catalyst during methanol oxidation indicates that Ir is likely serving a similar beneficial role as is Ru.

The effect of $Pt_{1.8}Ir$ catalyst drying temperature was also examined in this work. Figure 6 shows that the methanol oxidation activity is highest for films dried at ca. 250°C. At lower temperatures, it is conceivable that the $Pt_{1.8}Ir$ nanoparticulate film is still well dispersed, with some retained organics contributing to incomplete contact between the particles and the substrate. At drying temperatures >400°C, the activity drops significantly, perhaps due to particle sintering and the onset of conversion of Ir to IrOx.[15] The results of Fig. 6 mirror those obtained for pure Pt sols where the maximum CV current densities and H_{upd} charge densities are seen at drying temperature in the range of 200-250°C,[9] while the analogous optimum temperature for pure Ir sols is ~100°C.[10]

When the potential of bulk Ir electrodes is extended positively of 1.2 V *vs.* SHE, Ir undergoes an irreversible conversion to hydrous Ir oxide (IrOx).[25] At sol-derived Ir nanoparticles, we have reported[10] that these particles can be completely and irreversibly converted to IrOx by this means. To establish the impact of IrOx on methanol oxidation, similar to the debate as to whether Ru or Ru oxide is the active component of PtRu methanol oxidation catalysts, Au electrodes coated with $Pt_{1.8}Ir$ catalyst were cycled above 1.2 V *vs.* SHE until a steady-state CV was obtained. Evidence for the conversion of Ir to IrOx was obtained from the decrease in the size of the H_{upd} peaks, with the retained charge in these peaks attributed to the presence of Pt. Overall, ~25% of the UPD charge was lost due to IrOx formation, consistent with a surface composition of 1.8 Pt atoms (0.220 mC/cm^2) to 1 Ir atom (0.135 mC/cm^2). Furthermore, similar to $Pt_{1.8}Ir$, the $Pt_{1.8}IrOx$ signal was stable with cycling and showed no sign of CO poisoning.

Further evidence for the electrochemical formation of $Pt_{1.8}IrOx$ was obtained from the notable decrease in the methanol oxidation activity after extension to high potentials (Fig. 7, curve b) *vs.* the case before catalyst oxidation (Fig. 7, curve a). These results show that metallic $Pt_{1.8}Ir$ is the preferred form of the catalyst for methanol oxidation. The low methanol oxidation activity reported in the literature for previously studied Pt-Ir catalysts[12,13] may be because the oxidized form of Ir was present in these binary mixtures. This would be consistent with the high upper potentials and high drying temperature employed in previously published work.

Conclusions

Combining Pt and Ir sols together produces homogeneous catalysts mixed on the micrometer or sub-micrometer scale, with XRD and TEM analysis showing an average particle size of 2.5 ± 0.9 nm and with some indication of the formation of a Pt:Ir alloy. A 1:1 ratio of Pt:Ir in the individual starting materials resulted in a final product composition of 1.8 Pt to 1 Ir ($Pt_{1.8}Ir$), consistent with the fact that

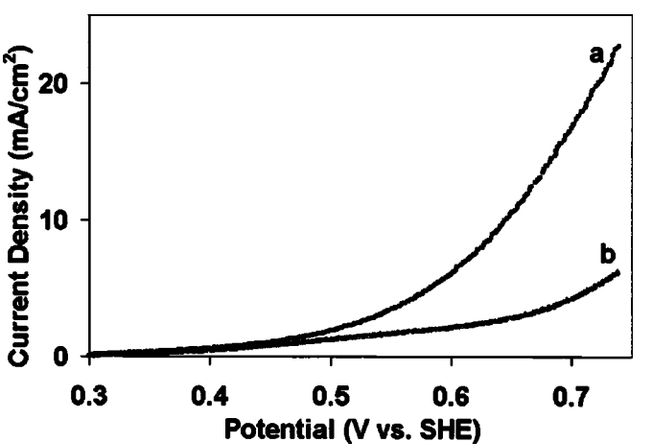

Figure 7. Methanol oxidation on (a) $Pt_{1.8}Ir$ formed at 200°C/15 min and (b) $Pt_{1.8}IrOx$, formed by the electrochemical oxidization of the electrode in (a). Corrected for geometric areas. (Stirred 1 M Methanol + 0.5 M H_2SO_4, 20 mV/s.)

some Ir was coprecipitated with NaCl during Ir sol synthesis. The CV response of $Pt_{1.8}Ir$ mixtures in 0.5 M sulfuric acid solutions, deposited on Au substrates, reveals a signature that appears more similar to Ir than Pt. These catalysts show excellent activity toward methanol oxidation at room temperature, with the activity commencing at ~0.275 V *vs.* SHE, and rivalling that observed with commercial supported PtRu catalysts. Furthermore, it was found that, on both a mass and true active area basis, the highest methanol oxidation activity was seen for $Pt_{1.8}Ir$ catalysts which were dried in air at ~250°C. At lower temperatures, interparticle bonding is likely not yet optimized, while higher drying temperatures may result in the thermal conversion of Ir to Ir oxide as well as particle sintering. When these $Pt_{1.8}Ir$ thin films were electrochemically converted to $Pt_{1.8}IrOx$, the methanol oxidation activity was greatly diminished, suggesting that the metallic state of Ir is the preferred form for catalysis. In addition, consistent with a surface composition of 1.8 Pt atoms (0.220 mC/cm^2) to 1 Ir atom (0.135 mC/cm^2), ~25% of the hydrogen UPD charge was lost due to the formation of IrOx in the binary catalyst.

Acknowledgments

We acknowledge the Natural Sciences and Engineering Research Council of Canada (NSERC) and the University of Calgary for the financial support of this work. Furthermore, we extend our thanks to Dr. H. Andreas and Dr. E. Abu Irhayem for valuable input on Pt and Ir sol synthesis.

The University of Calgary assisted in meeting the publication costs of this article.

References

1. P. Waszczuk, A. Wieckowski, P. Zelenay, S. Gottesfeld, C. Coutanceau, J.-M. Leger, and C. Lamy, *J. Electroanal. Chem.*, **511**, 55 (2001).
2. G. A. Camara, E. A. Ticianelli, S. Mukerjee, S. J. Lee, and J. McBreen, *J. Electrochem. Soc.*, **149**, A748 (2002).
3. J. W. Long, R. M. Stroud, K. E. Swider-Lyons, and D. R. Rolison, *J. Phys. Chem. B*, **104**, 9772 (2000).
4. S. C. Thomas, X. Ren, and S. Gottesfeld, *J. Electrochem. Soc.*, **146**, 4354 (1999).
5. H. N. Dinh, X. Ren, F. H. Garzon, P. Zelenay, and S. Gottesfeld, *J. Electroanal. Chem.*, **491**, 222 (2000).
6. P. Waszczuk, J. Solla-Gullón, H.-S. Kim, Y. Y. Tong, V. Montiel, A. Aldaz, and A. Wieckowski, *J. Catal.*, **203**, 1 (2001).
7. A. S. Arico, G. Monforte, E. Modica, P. L. Antonucci, and V. Antonucci, *Electrochem. Commun.*, **2**, 466 (2000).
8. D. R. Rolison, P. L. Hagans, K. E. Swider, and J. W. Long, *Langmuir*, **15**, 774 (1999).
9. H. A. Andreas and V. I. Birss, *J. Electrochem. Soc.*, **149**, A1481 (2002).
10. V. I. Birss, H. A. Andreas, I. Serebrennikova, and H. Elzanowska, *Electrochem. Solid-State Lett.*, **2**, 326 (1999).
11. I. Serebrennikova and V. I. Birss, *J. Electrochem. Soc.*, **144**, 566 (1997).
12. H. A. Andreas, H. Elzanowska, I. Serebrennikova, and V. I. Birss, *J. Electrochem. Soc.*, **147**, 4598 (2000).
13. H. A. Andreas, Ph.D. Thesis, University of Calgary (2003).
14. M. S. Ureta-Zanartu, P. Bravo, G. Reyes, C. Yanez, J. R. Gancedo, C. Gutierrez, and J. F. Marco, *Bol. Soc. Chil. Quim.*, **46**, 339 (2001).
15. A. Aramata, T. Kodera, and M. Masuda, *J. Appl. Electrochem.*, **18**, 577 (1988).
16. A. Hamnett and B. J. Kennedy, *Electrochim. Acta*, **33**, 1613 (1988).
17. R. M. Guppy and A. Atkinson, *Br. Ceram. Proc.*, **49**, 203 (1992).
18. P. Fang and Z. Wu, *Boli Yu Tangci*, **28**, 14 (2000).
19. H. A. Gasteiger, P. N. Ross Jr., and E. J. Cairns, *Surf. Sci.*, **293**, 67 (1993).
20. H. A. Gasteiger, N. Markovic, P. N. Ross Jr., and E. J. Cairns, *J. Phys. Chem.*, **97**, 12020 (1993).
21. D. A. Skoog and J. J. Leary, *Principles of Instrument Analysis*, 3rd ed., Harcourt Brace College Publishers, Toronto (1992).
22. R. Woods, in *Electroanalytical Chemistry*, Vol. 9, A. J. Bard, Editor, Marcel Dekker, New York (1976).
23. J. Mozota and B. E. Conway, *J. Electrochem. Soc.*, **128**, 2142 (1981).
24. D. A. J. Rand and R. Woods, *J. Electroanal. Chem.*, **55**, 375 (1974).
25. V. Birss, R. Myers, H. Angerstein-Kozlowska, and B. E. Conway, *J. Electrochem. Soc.*, **131**, 1502 (1984).